Surface & Coatings Technology 404 (2020) 126462

Contents lists available at ScienceDirect

Surface & Coatings Technology

journal homepage: www.elsevier.com/locate/surfcoat

Measurements and modeling of residual stress in sputtered TiN and ZrN: Dependence on growth rate and pressure

Zhaoxia Rao*, Eric Chason

School of Engineering, Brown University, Providence, RI 02912, USA

ARTICLE INFO

Keywords:
Thin films
Residual stress
Energetic deposition

ABSTRACT

In situ wafer curvature measurements have been conducted on sputter-deposited nitride films (TiN, ZrN) to investigate the effect of growth rate and pressure on stress. For each growth rate, the stress becomes more compressive at lower pressure. At high pressure the stress shows a weak dependence on growth rate, while at low pressure, it becomes more compressive at higher growth rates. The results are interpreted in terms of a kinetic model that includes the effects of growth kinetics and energetic particle bombardment. The overall agreement suggests that the model can reproduce the dependence on processing conditions in multiple nitride systems.

1. Introduction

Nitride-transition metal films are widely used due to their excellent mechanical properties and chemical inertness [1–4]. However, the deposited thin films are generally in a state of stress that can lead to cracks, delamination or deformation and affect their performance and reliability [5,6]. To modify the stress, sputter deposition is a popular method to deposit these films. A deeper understanding of the relationship between stress and processing conditions would be useful to enable the stress to be predicted under different sputtering conditions.

Although there have been many previous measurements [7–9] and references therein, they often only examine a limited range of processing conditions and/or do not fully characterize the corresponding microstructure. This makes it difficult to fully analyze the stress in order to understand the kinetic parameters controlling it. To address this, the current study aims to develop a comprehensive set of measurements that quantifies the dependence of stress on growth rate and pressure with grain size measurement for TiN and ZrN thin films. To determine the individual effects of the processing parameter, measurements are performed in which only one is varied while keeping the others constant.

The data is interpreted in terms of a previously-developed model [10] that relates the measured dependence on processing conditions to the underlying kinetic processes controlling it. Fitting the data to this model produces a set of parameters that allow the stress to be predicted under different conditions. This work is therefore part of a larger goal of being able to predict stress in different thin film materials under different processing conditions.

Sputter deposition is widely used to control stress in thin films [6,7,11–18]. The effects of multiple processing conditions have been investigated, including pressure [6,8,9,17,19–23], growth rate [24–26], grain size [27], substrate bias voltage [22,28–31], and N_2 gas flow rate [9,32]. The influence of gas pressure on residual stress in sputtered films has been well-studied [6,9]. A general observation is that the residual stress is more compressive at lower pressure, and more tensile at higher pressure. Thornton and Hoffman [6] identified a transition pressure below which the stress is compressive and above which the stress is tensile. The transition pressure has been determined to depend logarithmically on the atomic mass of the sputtered material so that heavier materials therefore reach a stress-free state at a higher pressure than lighter materials. The dependence of stress on pressure in TiN [9] and ZrN [8] has been reported. In TiN, the stress changes from −1.55 to 0.30 GPa with the increase of the pressure from 0.30 to 0.55 Pa, accompanied by a change of texture from (002) to (111). In ZrN, the stress changes from −6.5 to 0.40 GPa with the increase of pressure from 0.13 to 0.42 Pa. In both materials, the stress is made more compressive by the application of negative substrate bias voltage which increases the contribution of atomic peening. The (002) preferred orientation in TiN at lower pressure also correlates with a more compressive stress. In the current study, we limit the processing condition to a range in which the films have the same (111) preferred orientation.

For non-energetic growth (e.g., electrodeposition and evaporation) [33,34], the stress becomes more compressive at lower growth rate and more tensile at higher growth rate. For energetic deposition (e.g., sputtering deposition), however, a different dependence on growth rate is observed. In sputtered AlN [24,25], TaN [35], TiN [36] and Mo [37],

* Corresponding author.
E-mail address: zhaoxia_rao@brown.edu (Z. Rao).

https://doi.org/10.1016/j.surfcoat.2020.126462
Received 13 August 2020; Received in revised form 23 September 2020; Accepted 27 September 2020
Available online 03 October 2020

the stress becomes more compressive with the increase of growth rate at lower pressure. For higher mobility materials such as sputtered Cu [38], another stress turnaround is observed at low growth rates where the stress also becomes more compressive. This is attributed to the effects of film growth kinetics as well as energetic effects at lower pressure, as discussed in the kinetic model below.

Microstructural evolution is another important phenomenon that can affect stress evolution. The grain size at the surface has been shown to affect the stress in newly-deposited layers [34]. Grain growth within the film can also lead to additional stress [39]. Thornton [40] developed a zone structure model that summarizes the different types of microstructural evolution in sputtered materials depending on the deposition pressure and the temperature relative to melting temperature (T/T_m). For many metal-nitrides, the low atomic mobility means that the grain size does not change significantly during the film deposition.

To understand how the stress is related to the deposition conditions, a kinetic model has been developed that combines the effects of non-energetic film growth kinetics with those of energetic particle bombardment. This model has been previously applied to multiple studies of stress during energetic deposition (i.e., sputtered Mo [37] and Cu [38]) and non-energetic deposition (i.e., evaporated Ni [41] and electrodeposited Cu [42,43], Ni [34,44], and Co [45]). The physical basis of this model is reviewed in Section 3 and the results of fitting the model to the measurements are described in Section 5.

2. Materials and methods

In the experiments, nitride films were deposited onto [100] Si substrates by reactive DC magnetron sputtering deposition at ambient temperature. The dimension of Si substrate is 30 mm × 10 mm × 0.175 mm. The substrates were electrically grounded. Before deposition, the Si wafer was cleaned in successive baths of acetone, methanol, iso-propanol via ultrasonic agitation for 5 min each followed by drying with compressed nitrogen gas. The films were deposited from a 3″ diameter Ti target with purity of 99.995% and a 3″ diameter Zr target with purity of 99.2%. The target-substrate distance is 18 cm. There is no applied substrate bias voltage. Before introducing the reactive N_2 gas into the process chamber, a pre-cleaning of the target surface was performed in pure Ar gas atmosphere at a flow rate of 15 sccm (standard cubic centimeter per minute) for 10 min to remove contaminations on the target surface. The nitride films were deposited under a mixed Ar and N_2 atmosphere. The flow rate of Ar was kept at 26 sccm and the flow rate of N_2 was kept at 6 sccm for TiN and ZrN. The pumping speed was varied via a throttle valve to control the total gas pressure in the chamber. The deposition power (growth rate), and pressure were varied in the growth layers to investigate the dependence of stress evolution on the processing conditions. For TiN, the processing pressure (total gas pressure of Ar and N_2) was varied from 0.13 to 0.40 Pa, and the applied power was varied from 80 to 331 W with the growth rate changes from 0.009 to 0.124 nm/s, the corresponding target voltage changes from 393 to 472 V. For ZrN, the processing pressure was changed from 0.13 to 0.67 Pa, and the applied power was changed from 92 to 299 W with the growth rate changes from 0.042 to 0.187 nm/s, the corresponding target voltage changes from 395 to 520 V. The total film thickness in the measurements is no more than 920 nm.

The real-time stress evolution during film deposition was measured by a wafer curvature setup that was mounted onto the outside of the sputtering system. In this approach, a laser beam passes through an etalon, generating parallel beams which go through a quartz window at the chamber bottom to hit the sample. The reflected beams are measured by a CCD camera also mounted outside the chamber [46]. The curvature evolution is determined from the measured change in the spacing of the reflected laser beams. The resolution of the MOSS system used in this work is $5.68 \times 10^{-4}\ m^{-1}$, giving a sensitivity of 1.02 N/m for a (100) Si wafer substrate with a thickness of 100 μm.

The measured curvature is related to the film's stress and thickness by Stoney's equation [47]:

$$\kappa = \frac{6\overline{\sigma} h_f}{M_s h_s^2} \tag{1}$$

where $\overline{\sigma}$ is the average stress in the film and h_f and h_s are the film thickness and substrate thickness, respectively. M_s is the biaxial modulus of substrate. The product $\overline{\sigma} h_f$ is often referred to as the stress-thickness or force per width (F/w). The stress-thickness is obtained by averaging the stress in the thin film through its thickness:

$$\overline{\sigma} h_f = \int_0^{h_f} \sigma(z)\mathrm{d}z \tag{2}$$

where z is the direction normal to the substrate and $\sigma(z)$ is the in-plane stress at height z above the film/substrate interface. If there is no change in the stress of the underlying layers, the stress in new layers being deposited on the film surface (σ_{inc} or incremental stress) can be determined from the slope of the stress-thickness vs. thickness. If the grain size does not change with thickness, the incremental stress reaches a constant value that is referred to as the steady-state stress.

During the deposition, the growth rate and film thickness were monitored by a quartz crystal sensor. The actual film thickness was examined by JA Woollam ellipsometer and further confirmed by measurements from FEI CM20 Transmission Electron Microscopy (TEM). The films were analyzed by a Bruker D8 Discovery High resolution X-ray diffractometer (XRD) which confirmed they all had a cubic crystal structure with a preferred (111) orientation as shown in Fig. 1. The cross-sectional microstructure of the films was characterized using TEM on cross-sections made by a FEI Helios focused ion beam (FIB).

In order to evaluate the energetic effects of incoming particles, a combination of Monte-Carlo simulations (SRIM [48] and SIMTRA [49]) were performed to compute the average energy of the incoming particles arriving at the substrate. First, the sputter yield, initial energy and angular distribution of sputtered atoms and backscattered neutrals at the target were obtained from SRIM. The incident energy of Ar^+ ions was set as 75% of the target discharge voltage due to charge transfer collision in the plasma sheath [50]. The average discharge voltage is used to estimate the initial energy of the Ar ions. Simulations using the individual discharge voltages for each data set show that the average energy per sputtered atom and the ratio of the flux of backscattered neutrals to the flux of sputtered atoms have only a weak dependence on growth rate, so using the average discharge voltage is adequate. The simulations for Ti and Zr target were performed using 6×10^5 Ar^+ ions with energy of 340 eV. The atomic displacement energy for Ti and Zr are 30 and 40 eV as reported by Lucasson [51], respectively. The calculated sputter yield from Ti and Zr targets are 0.47 and 0.59, and the backscattered yield from Ti and Zr targets are 0.03 and 0.13. Second, the initial energy and angular distribution of particles at the target was used as input to SIMTRA to simulate the transport of particles in a vacuum chamber with similar geometry as the experimental environment. The average energy of the arriving particles per sputtered atom is calculated as $E_{avg} = E_s + \alpha E_b$, where E_s is the average energy for sputtered atoms and E_b is the average energy for backscattered neutrals, and α refers to the ratio of the flux of backscattered neutrals to the flux of sputtered atoms. Based on the average energy of each energetic particles at each pressure, the implantation depth for each particle at each pressure was calculated in SRIM. The average energy per sputtered atom and the weighted average implantation depth of the arriving particles at each pressure are tabulated in Table 1.

3. Theory/calculation

In order to understand the effects on stress observed for the different processing conditions, we invoke a kinetic model that has been described previously [10]. Only a brief description of the model is given here; further details can be found in the original publication. The

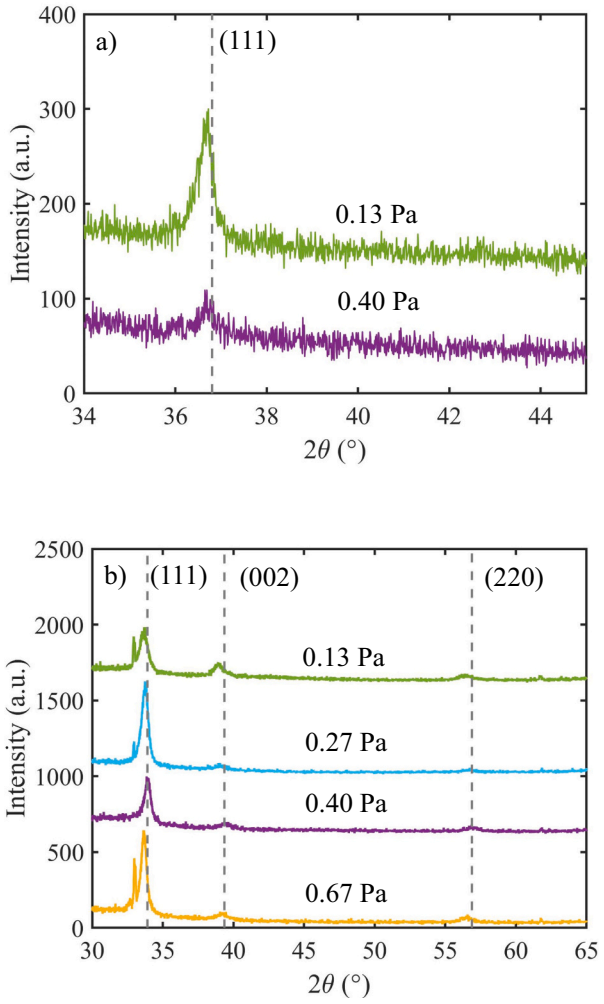

Fig. 1. XRD patterns for a) TiN and b) ZrN grown with multiple growth rates at different pressures with thicknesses in the range of 580–920 nm.

Table 1
Average particle energy and implantation depth calculated using SIMTRA and SRIM for different pressures.

Pressure (Pa)	Average energy per deposited atom at substrate (eV)		Weighted average implantation depth (nm)	
	TiN	ZrN	TiN	ZrN
0.13	15.45	35.50	0.34	0.40
0.27	N/A	25.43	N/A	0.30
0.40	5.42	15.28	0.19	0.28
0.67	N/A	5.34	N/A	0.16

kinetic model is comprised of two parts that are considered additive: the effect of growth kinetics during non-energetic growth (electrodeposition or evaporation) and the additional stress induced by the effect of energetic particles.

The growth model focuses on the stress generated at the top of the grain boundary (triple junction) that forms between adjacent islands as the film grows. It considers a dynamic competition between tensile and compressive stress generating processes. The tensile stress is based on a mechanism originally proposed by Hoffman [52]. Layers will develop stress during island coalescence as long as the reduction in interfacial energy is more than the gain in elastic strain energy. It predicts that the tensile stress, σ_T, is dependent on $(M_f \Delta\gamma/L)^{1/2}$, where M_f is the biaxial modulus of the film, $\Delta\gamma$ is the difference in interfacial energy between the surface and grain boundary and L is the grain size in the film.

The compressive stress is assumed to arise from adatoms on the surface diffusing into the grain boundary driven by the non-equilibrium conditions on the growing film surface [53]. These two mechanisms are combined into a rate equation which relates the incremental to the effective diffusivity, grain size (L) and growth rate (R):

$$\sigma_{growth} = \sigma_C + (\sigma_T - \sigma_C)e^{-\frac{\beta D}{RL}} \tag{3}$$

σ_C is the limiting compressive stress due to the surface conditions and βD is a kinetic parameter based on the transition rate between atoms on the surface and the grain boundary. The model can be extended to consider the effect of grain growth in the film [41], but that is left out of Eq. (3) since it is not relevant for the measurements described here.

Additional terms have been developed to describe the effects of energetic particles on stress evolution:

$$\sigma_{energetic} = A_0\left(\frac{l}{L}\right) + \left(1 - \frac{l}{L}\right)\frac{B_0}{1 + \frac{l}{R\tau_s}} \tag{4}$$

where l is the average depth of the defects created by the energetic particles. The first term on the right-hand side models the effect of collision-induced densification near the grain boundary [54]. It depends on l/L because it is assumed to occur in the region of the grain within one implantation depth l from the grain boundary. A_0 is an adjustable parameter which depends on the pressure and the ratio of the flux of energetic particles to the deposition rate.

The second term on the right-hand side models stress generated by the incorporation of the defects in the remainder of the film (proportional to $\left(1 - \frac{l}{L}\right)$). It is assumed to be proportional to the number of defects retained in the bulk during deposition. B_0 is an adjustable parameter that depends on the number of defects created per incident particle and the corresponding stress per defect. τ_s is the characteristic time it takes for a defect implanted at depth l to diffuse to the surface. Since the surface is moving up at a rate of R, the diffusion distance equals to the distance to the moving surface as

$$\sqrt{D_i \tau_s} = l + R\tau_s \tag{5}$$

where D_i is the diffusivity of sputter-induced defects.

The stress generating effects of growth kinetics and energetic bombardment are assumed to be additive [10,55]. Putting Eqs. (3) and (4) together produces a comprehensive kinetic model that predicts the stress for different processing conditions. To compare the experimental results with the kinetic model, a non-linear least squares fitting routine is used to obtain the optimal parameters that minimize the residual between the model and the measurements of the steady-state stress. For the parameters σ_C, σ_T, βD, D_i, a single value of each is used to simultaneously fit all the measurements for each material as these parameters are not expected to change with growth rate or pressure.

The other parameters (A_0, B_0, l) are expected to depend on the pressure. To reduce the number of free parameters, these parameters in each material are assumed to have a linear dependence on P so that $A_0 = \left(1 - \frac{P}{P_0}\right)A^*$, $B_0 = \left(1 - \frac{P}{P_0}\right)B^*$ and $l = \left(1 - \frac{P}{P_0}\right)l^*$ where P_0 is a threshold pressure for each material. The energetic effects are assumed to be negligible when the pressure is above the threshold pressure. Based on TEM measurements, the grain size was assumed to be 50 nm in both materials for all conditions.

4. Results

As described in the Introduction section, stress in nitride films depends on multiple parameters (e.g., growth rate, grain size, pressure) whose interactions are complex. For instance, changing the growth rate can change the grain size so it is not immediately clear which is responsible for the stress change. To advance our understanding, experiments need to be designed so that the effects of each parameter can be determined separately.

Therefore, a series of measurements were performed for different growth rates while keeping the pressure constant at several different values. The same growth rates were also measured at different pressures. This showed that a single value of the steady-state stress could be associated with each growth rate and pressure. For each set of measurements, a buffer layer with nominal thickness of 100 nm was initially deposited so that all the subsequent measurements were done on the same starting surface. A buffer layer of TiN was grown at a growth rate of 0.089 nm/s and a pressure of 0.13 Pa for TiN and a buffer layer of ZrN was grown at a growth rate of 0.085 nm/s and a pressure of 0.40 Pa for ZrN. The grain size was estimated to be fairly constant during the growth based on the relatively constant slope of the curvature measurements with thickness and its repeatability for the same growth rate at different thicknesses. A changing grain size would lead to a changing slope of the curvature measurements [41]. In addition, stress relaxation during growth interrupts is minimal. The grain sizes of the columnar structure in TiN and ZrN were estimated to be 50 nm from TEM images although it was difficult to determine and the estimates may have significant error. For comparison, Abadias et al. [7] also reported that there is no stress relaxation during the growth interrupt in TiN and ZrN at 300 °C, and the measured grain sizes in their work are ~30 nm and ~23 nm for TiN and ZrN, respectively. The measured grain size of TiN deposited on stainless steel substrates without substrate heating is in the range of 50–100 nm as reported by Banerjee et al. [56]. The sequence of experiments and the corresponding results are described below.

4.1. Continuous growth at single rate

A series of stress-thickness measurements for continuous ZrN films deposition at 0.085 nm/s and different pressures is shown in Fig. 2. The stress evolution in the buffer layer which was grown at pressure of 0.40 Pa and a growth rate of 0.085 nm/s is similar for all the measurements, showing that the reproducibility is good. After the buffer layer growth, the pressure was changed to values from 0.13 to 0.67 Pa, as indicated in the figure. The slope of the stress-thickness rapidly reaches a constant value that corresponds to the steady-state incremental stress. The constancy of the slope implies that the grain size does not change significantly during the film growth. At lower pressures, the stress is more compressive and changes from compressive to tensile with the increase of pressure. However, the results at 0.40 and 0.67 Pa are very similar which suggests that the stress becomes less dependent on pressure when the pressure is high.

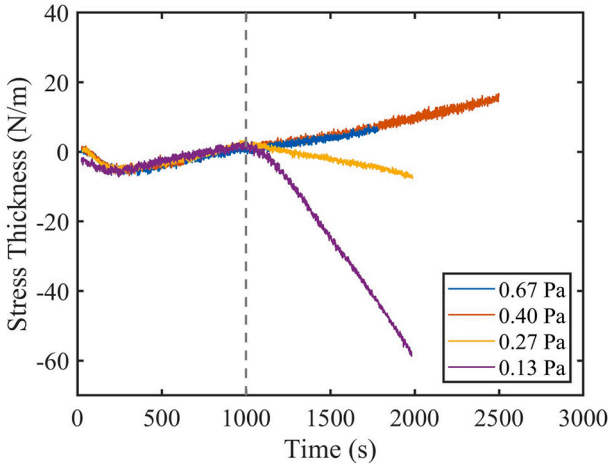

Fig. 2. Wafer curvature measurements of stress-thickness evolution in sputter-deposited ZrN at a rate of 0.085 nm/s and the pressure indicated in the figure. For each film, a nominal 100 nm buffer layer was first grown at 0.40 Pa to make the starting surface identical. The dashed vertical line indicates the transition point from buffer layer to growth layer.

4.2. Multiple growth sequences at different rates

Since the change in grain size with thickness is not significant, it is possible to measure the dependence on growth rates by performing sequences of growth at different rates on the same sample. The stress-thickness is measured at one rate for a period long enough to determine the slope and hence the incremental stress. This is followed by a pause while the growth rate is changed and then subsequent growth at the new growth rate. For each material, the same conditions are used for the first nominal thickness of 100 nm of growth (buffer layer described above) in order to make the initial grain size and texture the same for all the measurements. This approach has been used previously in electrodeposited Cu and Ni [42,44] and makes it possible to efficiently study the effect of different growth conditions without having to prepare a new sample for each measurement. The sequence includes multiple measurements at each growth rate to confirm that the stress depends only on the growth rate and does not change with thickness. This also enables the experimental error (standard deviation) in each measurement to be determined. The same approach is repeated at different growth pressures in order to obtain a comprehensive set of measurements of stress vs. growth rate and pressure.

A sequence of growths for ZrN films at multiple rates and a pressure of 0.13 Pa (after the buffer layer growth) is shown in Fig. 3. The growth rate for each interval is shown in Fig. 3a and the stress-thickness in Fig. 3b. After each growth sequence, the deposition was paused for at least 3 min to determine if there was any stress relaxation before the growth was resumed at another rate. The stress during the pauses (shown by the shaded areas in Fig. 3) does not change significantly, indicating the stress relaxation is minimal. The growth rates were repeated to determine whether the stress changes with film thickness (for instance, due to change in the grain size with thickness). In general, the repeated stress is the same or only slightly more compressive than the previous growth stress, which indicates that any effects of grain growth are small. This approach was used at other pressures to develop a comprehensive set of stress-thickness measurements for ZrN and TiN at different growth rates and pressures.

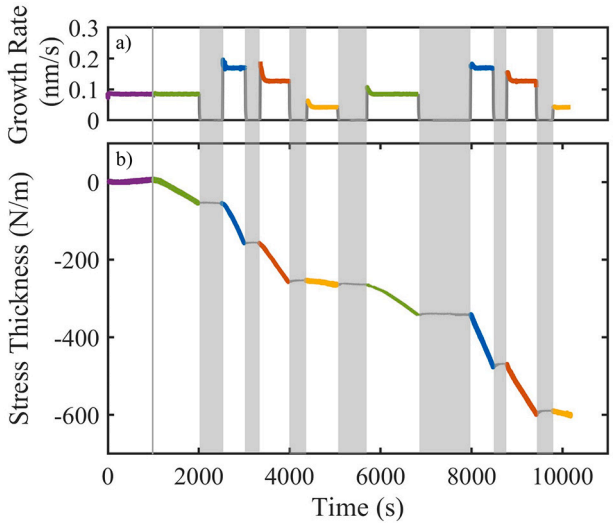

Fig. 3. Sequential measurements of stress evolution in ZrN deposited at 0.13 Pa grown at different growth rates. a) Growth rate corresponding to different intervals of growth b) stress-thickness evolution at different growth rates. The gray areas correspond to pauses while the growth rate was changed. The buffer layer was grown at 0.40 Pa to make the starting surface the same as other measurements.

4.3. Steady-state stress in nitride films for different growth rates and pressures

The steady-state stress was determined from the slopes of the stress-thickness measurements. The results are shown for TiN and ZrN, in Fig. 4a, and b, respectively. Note that the axes for the stress are different in each case. The solid lines in the figure are the fits from a kinetic model which has been described in Section 3.

The error bars in the figure were obtained by taking the standard deviation of repeated experimental measurements at each deposition condition. On average, the standard deviation from multiple measurements on each sample is 10.3 MPa for TiN and 13.0 MPa for ZrN. For measurements taken on different samples, we can look at the standard deviation of the multiple measurements of the buffer layer stress which is 17.4 MPa for TiN and 9.6 MPa for ZrN. The similarity in the determinations of the errors shows that changing the sample does not introduce a large amount of additional error. In either case, the error on the stress determination is not large compared to the change in stress with growth rate and pressure.

Some important trends can be identified in the results. In each film, the stress is more compressive for the same growth rate at lower pressure. For each pressure, the stress becomes more compressive at higher growth rate with a stronger growth-rate dependence at low pressure. Comparing the two materials, at high pressure the stress in ZrN is similar to TiN with a tensile value that is weakly dependent on the growth rate. At lower pressure, however, the stress in ZrN is more compressive than TiN and the growth rate dependence is more pronounced.

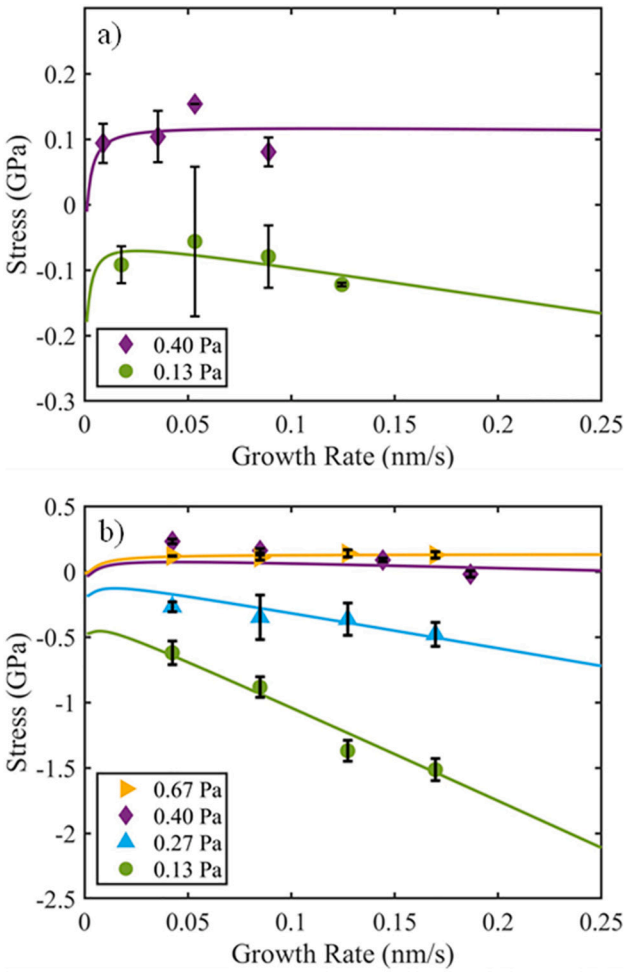

Fig. 4. Steady-state stress vs. growth rate at different pressures for a) TiN and b) ZrN.

5. Discussion

The trends in the steady-state stress with pressure and growth rate shown in Fig. 4 are consistent with measurements seen previously in other sputtered films [37,38]. The dependence of the stress on pressure has been attributed to a change in the energy of the incoming particles. At low pressure, the energetic particles induce compressive stress due to densification at the grain boundaries and defect-production [10,54]. In this regime, higher growth rates tend to create more compressive stress. This is the opposite of what is seen for non-energetic growth in which higher growth rates tend to make the stress less compressive/more tensile [33,34] and, for low mobility materials, ultimately saturate at a tensile value. This type of behavior is seen for both TiN and ZrN at high pressure and correspondingly low energy. The tensile stress at higher pressure has been attributed to the existence of voids in the film as the film density decreases with the increase of pressure [8] though it may also be related to island coalescence. In the ZrN films, it can be seen that reducing the pressure from 0.67 to 0.40 Pa has little effect on the stress. This suggests that at sufficiently high pressures, the energy of sputtered atoms and backscattered neutrals is reduced to a point where the energetic contributions to the stress are small.

Additional understanding of the processes contributing to stress can be gained by looking at the results of fitting the data to the kinetic model. The solid lines in Fig. 4 show the calculated stress using the parameters obtained from the fitting. The model is able to capture both the pressure and growth rate dependence for each material. The corresponding fitting parameters are shown in Table 2; the values of A_0, B_0 and l calculated from these parameters at the measured pressures are shown in Table 2b. Note that these parameters represent values that make the model agree most closely with the data. But since the disagreement is not only due to experimental error, we cannot statistically determine the error associated with each value of the parameters. Additionally, physical approximations made in the model means that care should be taken in interpreting their exact values. Nevertheless, it is instructive to compare the fitting parameters with estimates from the materials properties to explore the validity of the model and to shed light on the underlying processes controlling the stress.

According to the fitting, the value of the tensile stress parameter σ_T is the same for Ti and Zr. For comparison, Hoffman's mechanism [52] proposes that σ_T is proportional to $\sqrt{M_f \Delta\gamma / L}$ where $\Delta\gamma$ is the interfacial energy difference between the free surface and the grain boundary. Although we do not know the values of $\Delta\gamma$ for these materials, for comparison we assume that the value is proportional to the melting point of each material (3220 and 3225 K for TiN and ZrN, respectively), the film modulus with (111) preferred orientation (550 GPa [57] for TiN and 460 GPa [58] for ZrN) and assuming the same grain size. This predicts a difference of only 9% between the materials. Therefore, the relative values calculated from Hoffman's model are consistent with the similarity found for the fitting values.

The values of the kinetic parameter βD are 0.12 and 0.19 nm^2/s for TiN and ZrN, respectively. Because the concentration of mobile surface atoms is not known, βD cannot be calculated from other measurements such as the surface diffusivity. This parameter controls the transition from tensile to compressive stress as the growth rate is decreased due to non-energetic growth processes. With the conditions accessible in this study, a transition to compressive stress could not be observed in the measurements at low growth rates. Therefore, the value obtained from the fitting for this parameter is likely an overestimate. For comparison, measurements of sputtered Cu [38] do show a tendency for the stress to become more compressive at the lower range of growth rates used in this study. The value of βD obtained for sputtered Cu is 0.67 nm^2/s which is larger than for TiN or ZrN, suggesting that the surface mobility of Cu atoms is higher than in the nitrides.

To evaluate the parameters corresponding to energetic processes, the average energy per sputtered atom at the substrate is computed from Monte-Carlo simulations (SRIM and SIMTRA). Results for TiN and

Table 2
a) Parameters determined from fitting the data to the kinetic model. b) Values of fitting parameters at different pressures assuming a linear pressure dependence described in text.

	σ_c (GPa)	σ_T (GPa)	βD (nm^2/s)	D_i (nm^2/s)	P_0 (Pa)	A^* (GPa)	B^* (GPa)	l^* (nm)
TiN	−0.02	0.11	0.12	9.87	0.47	−55.93	−25.35	0.27
ZrN	−0.10	0.11	0.19	3.52	0.48	−226.04	−234.08	0.17

	Pressure (Pa)	A_0 (GPa)	B_0 (GPa)	l (nm)
TiN	0.13	−40.36	−18.29	0.20
…	0.40	−8.03	−3.64	0.04
ZrN	0.13	−164.82	−170.68	0.12
…	0.27	−98.89	−102.41	0.07
…	0.40	−37.67	−39.01	0.03

ZrN at different pressures are shown in Fig. 5. Over the pressure range examined, the average energy decreases with increasing pressure; a linear fit to the data is indicated by the dashed lines. The energy per particle is larger for ZrN relative to TiN growth at the same pressure. For comparison, the magnitudes of the energetic parameters A^* and B^* (Table 2) are also larger for ZrN than for TiN. The intercepts of the lines with the x-axis are an estimate of the threshold pressure at which the average energy goes to zero. It is similar for the two materials which is consistent with the values of the threshold pressure (P_0) from the fitting, although the value obtained from the fitting is smaller.

The average implantation depth of each material was calculated by taking the weighted average of implantation depth of each energetic particle. The implantation depth was calculated by using SRIM. For input, SIMTRA was used to estimate the energy range of the incoming particles at different pressures. The average particle energy and corresponding implantation depth are shown in Table 1 for each material and pressure. The implantation depth decreases with increasing pressure in both materials. The maximum implantation depth at 0.13 Pa in TiN is 0.34 nm while that in ZrN is 0.40 nm. For comparison, the values of l from the fitting produce 0.12 nm for TiN and 0.20 nm for ZrN. We consider the fact that they only differ by less than a factor of two to be relatively good agreement.

The fitting parameter for the sputter-induced defect diffusivity (D_i) has a value of 9.87 nm^2/s in TiN and 3.52 nm^2/s in ZrN. For comparison, this value for TiN is significantly higher than diffusivity estimates for point defects in TiN of 10^{10} nm^2/s at temperature of 2500 K [59–61]. These studies also suggest that interstitial diffusion is much faster than vacancies which suggests that interstitials may be the dominant mobile defect that controls the stress evolution kinetics. However, there is still a wide discrepancy between the fitting parameter needed to explain the growth-rate dependent stress and other measurements of defect diffusivity. This may indicate that other processes such as stress-enhanced diffusion play a role.

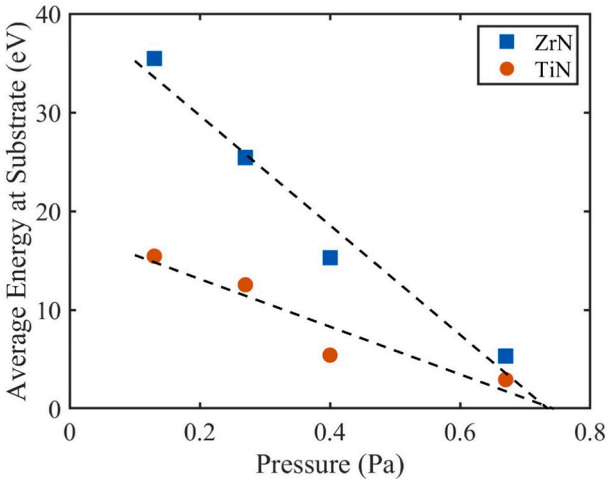

Fig. 5. Average energy per particle vs. pressure estimated using SIMTRA and SRIM for ZrN and TiN.

Because the data was taken at only one temperature and a constant grain size, the fitting does not provide any information about the activation energy for diffusion or the grain size dependence of the kinetics in the model. Further experiments that study the grain size and temperature dependence are needed to probe these issues. Experiments for other metal nitrides would also be useful to determine whether the model parameters are consistent with the physical properties of materials for a wider range of elements. The ultimate goal of this work would be to develop a quantitative model that can predict the stress in different materials for different processing conditions.

6. Conclusions

We conducted experiments to explore the effect of growth rate and pressure on residual stress in sputtering deposited TiN and ZrN films. The results show that the stress is more tensile at higher pressure and more compressive at lower pressure. At higher pressure, the stress is weakly dependent on growth rate, but at lower pressure, the stress is more compressive with the increase of growth rate. This behavior is consistent with a kinetic model that includes contributions from the growth kinetics and energetic particle bombardment during sputtering deposition. The parameters obtained from fitting the model to the data have values that are physically reasonable. The parameters governing the tensile stress generated by island coalescence are similar, as expected from evaluating the model proposed by Hoffman. The energetic parameters are consistent with estimates made using Monte-Carlo simulations SRIM and SIMTRA. The apparent consistency between the prediction of the model and the experimental results supports the validity of the mechanisms used in the model.

CRediT authorship contribution statement

Zhaoxia Rao: performed the experiments, analyzed the data and wrote the manuscript.

Eric Chason: directed the research, contributed to the discussion and interpretation of the results, and reviewed and edited the manuscript.

Declaration of competing interest

The authors declare that they have no known competing financial interests or personal relationships that could have appeared to influence the work reported in this paper.

Acknowledgements

This work was supported by the National Science Foundation (NSF) under Contracts No. DMR-1602491 and DMR-2006422.

Appendix A. Supplementary data

Supplementary data to this article can be found online at https://doi.org/10.1016/j.surfcoat.2020.126462.

References

[1] S.Q. Wang, I. Raaijmakers, B.J. Burrow, S. Suthar, S. Redkar, K.B. Kim, J. Appl. Phys. 68 (1990) 5176–5187.
[2] M.B. Takeyama, A. Noya, K. Sakanishi, J. Vac, Sci. Technol. B 18 (2000) 1333–1337.
[3] J.-S. Chun, I. Petrov, J.E. Greene, J. Appl. Phys. 86 (1999) 3633–3641.
[4] A.E.K., E. Eisenbraun, Annu. Rev. Mater. Sci. 30 (2000) 363–385.
[5] A.J. Perry, J. Vac, Sci. Technol. A 8 (1990) 1351–1358.
[6] J.A. Thornton, D.W. Hoffman, Thin Solid Films 171 (1989) 5–31.
[7] G. Abadias, P. Guerin, Appl. Phys. Lett. 93 (2008) 111908.
[8] L.E. Koutsokeras, G. Abadias, J. Appl. Phys. 111 (2012) 093509.
[9] G. Abadias, W.P. Leroy, S. Mahieu, D. Depla, J. Phys. D. Appl. Phys. 46 (2012) 055301.
[10] E. Chason, M. Karlson, J.J. Colin, D. Magnfält, K. Sarakinos, G. Abadias, J. Appl. Phys. 119 (2016) 145307.
[11] H. Windischmann, Crit. Rev. Solid State Mater. Sci. 17 (1992) 547–596.
[12] P.M. Fabis, R.A. Cooke, S. McDonough, J. Vac. Sci. Technol. A 8 (1990) 3809–3818.
[13] G. Abadias, Surf. Coat. Technol. 202 (2008) 2223–2235.
[14] G. Abadias, E. Chason, J. Keckes, M. Sebastiani, G.B. Thompson, E. Barthel, G.L. Doll, C.E. Murray, C.H. Stoessel, L. Martinu, J. Vac. Sci. Technol. A 36 (2018) 020801.
[15] G. Abadias, L.E. Koutsokeras, A. Siozios, P. Patsalas, Thin Solid Films 538 (2013) 56–70.
[16] G. Abadias, Y.Y. Tse, P. Guérin, V. Pelosin, J. Appl. Phys. 99 (2006) 113519.
[17] Y.G. Shen, Mater. Sci. Eng. A 359 (2003) 158–167.
[18] Y.G. Shen, Y.W. Mai, D.R. McKenzie, Q.C. Zhang, W.D. McFall, W.E. McBride, J. Appl. Phys. 88 (2000) 1380–1388.
[19] C.T. Wu, Thin Solid Films 64 (1979) 103–110.
[20] J.A. Thornton, J. Tabock, D.W. Hoffman, Thin Solid Films 64 (1979) 111–119.
[21] E.A.I. Ellis, M. Chmielus, S.P. Baker, Acta Mater. 150 (2018) 317–326.
[22] A.J. Detor, A.M. Hodge, E. Chason, Y. Wang, H. Xu, M. Conyers, A. Nikroo, A. Hamza, Acta Mater. 57 (2009) 2055–2065.
[23] G. Abadias, L.E. Koutsokeras, P. Guerin, P. Patsalas, Thin Solid Films 518 (2009) 1532–1537.
[24] H.Y. Liu, G.S. Tang, F. Zeng, F. Pan, J. Cryst. Growth 363 (2013) 80–85.
[25] K. Kusaka, D. Taniguchi, T. Hanabusa, K. Tominaga, Vacuum 59 (2000) 806–813.
[26] A. Jamnig, N. Pliatsikas, K. Sarakinos, G. Abadias, J. Appl. Phys. 127 (2020) 045302.
[27] D. Magnfält, A. Fillon, R.D. Boyd, U. Helmersson, K. Sarakinos, G. Abadias, J. Appl. Phys. 119 (2016) 055305.
[28] J. Lin, W.D. Sproul, J.J. Moore, Z.L. Wu, S.L. Lee, J. Phys. D. Appl. Phys. 44 (2011) 425305.
[29] H.-C. Lee, J.-Y. Lee, H.-J. Ahn, Thin Solid Films 251 (1994) 136–140.
[30] A.M. Engwall, S.J. Shin, J. Bae, Y.M. Wang, Surf. Coat. Technol. 363 (2019) 191–197.
[31] F. Cemin, G. Abadias, T. Minea, C. Furgeaud, F. Brisset, D. Solas, D. Lundin, Acta Mater. 141 (2017) 120–130.
[32] B. Subramanian, K. Prabakaran, M. Jayachandran, Bull. Mater. Sci. 35 (2012) 505–511.
[33] S.J. Hearne, J.A. Floro, J. Appl. Phys. 97 (2005) 014901.
[34] A.M. Engwall, Z. Rao, E. Chason, Mater. Des. 110 (2016) 616–623.
[35] C.-T. Wei, H.-P.D. Shieh, Jpn. J. Appl. Phys. 45 (2006) 6405–6410.
[36] C. Saringer, R. Franz, K. Zorn, C. Mitterer, J. Vac. Sci. Technol. A 34 (2016) 041517.
[37] A. Fillon, G. Abadias, A. Michel, C. Jaouen, Thin Solid Films 519 (2010) 1655–1661.
[38] T. Kaub, Z. Rao, E. Chason, G.B. Thompson, Surf. Coat. Technol. 357 (2019) 939–946.
[39] H.Z. Yu, C.V. Thompson, Acta Mater. 67 (2014) 189–198.
[40] J.A. Thornton, J. Vac. Sci. Technol. 11 (1974) 666–670.
[41] E. Chason, A.M. Engwall, Z. Rao, T. Nishimura, J. Appl. Phys. 123 (2018) 185305.
[42] A.M. Engwall, Z. Rao, E. Chason, J. Electrochem. Soc. 164 (2017) D828–D834.
[43] E. Chason, A. Engwall, F. Pei, M. Lafouresse, U. Bertocci, G. Stafford, J.A. Murphy, C. Lenihan, D.N. Buckley, J. Electrochem. Soc. 160 (2013) D3285–D3289.
[44] Z. Rao, S.J. Hearne, E. Chason, J. Electrochem. Soc. 166 (2018) D3212–D3218.
[45] V.P. Graciano, U. Bertocci, G.R. Stafford, J. Electrochem. Soc. 166 (2019) D3246–D3253.
[46] E. Chason, P.R. Guduru, J. Appl. Phys. 119 (2016) 191101.
[47] G.G. Stoney, Proc. R. Soc. Lond. A 82 (1909) 172–175.
[48] J.F. Ziegler, J.P. Biersack, U. Littmark, The Stopping and Range of Ions in Matter, Springer, Boston, MA, 1985.
[49] K. Van Aeken, S. Mahieu, D. Depla, J. Phys. D. Appl. Phys. 41 (2008) 205307.
[50] A. Bogaerts, I. Kolev, G. Buyle, Modeling of the magnetron discharge, in: D. Depla, S. Mahieu (Eds.), Reactive Sputter Deposition, Springer, Berlin, 2008, pp. 61–130.
[51] P. Lucasson, Fundamental aspects of radiation damage in metals, Proceedings of International Conference at Gatlinburg, Tennessee, 1975, p. 42.
[52] R.W. Hoffman, Thin Solid Films 34 (1976) 185–190.
[53] E. Chason, B.W. Sheldon, L.B. Freund, J.A. Floro, S.J. Hearne, Phys. Rev. Lett. 88 (2002) 156103.
[54] D. Magnfält, G. Abadias, K. Sarakinos, Appl. Phys. Lett. 103 (2013) 051910.
[55] G.C.A.M. Janssen, J.-D. Kamminga, Appl. Phys. Lett. 85 (2004) 3086–3088.
[56] R. Banerjee, K. Singh, P. Ayyub, M.K. Totlani, A.K. Suri, J. Vac. Sci. Technol. A 21 (2003) 310–317.
[57] D.S. Stone, K.B. Yoder, W.D. Sproul, J. Vac. Sci. Technol. A 9 (1991) 2543–2547.
[58] E. Török, A.J. Perry, L. Chollet, W.D. Sproul, Thin Solid Films 153 (1987) 37–43.
[59] F. Elstner, H. Kupfer, F. Richter, Phys. Status Solidi A 147 (1995) 373–377.
[60] L. Hultman, Vacuum 57 (2000) 1–30.
[61] D. Gambino, Titanium Vacancy Diffusion in TiN via Non-equilibrium Ab Initio Molecular Dynamics, Master thesis Linkoping University, 2016.